arTs Università degli Studi di Trieste
Archivio della ricerca – postprint

Alkali metals in white dwarf atmospheres as tracers of ancient planetary crusts

Mark A. Hollands[1]✉, Pier-Emmanuel Tremblay[1], Boris T. Gänsicke[1,2], Detlev Koester[3] and Nicola Pietro Gentile-Fusillo[4]

White dwarfs that accrete the debris of tidally disrupted asteroids[1] provide the opportunity to measure the bulk composition of the building blocks, or fragments, of exoplanets[2]. This technique has established a diversity of compositions comparable to what is observed in the Solar System[3], suggesting that the formation of rocky planets is a generic process[4]. The relative abundances of lithophile and siderophile elements within the planetary debris can be used to investigate whether exoplanets undergo differentiation[5], yet the composition studies carried out so far lack unambiguous tracers of planetary crusts[6]. Here we report the detection of lithium in the atmospheres of four cool (<5,000 K) and old (cooling ages of 5–10 Gyr ago) metal-polluted white dwarfs, of which one also displays photospheric potassium. The relative abundances of these two elements with respect to sodium and calcium strongly suggest that all four white dwarfs have accreted fragments of planetary crusts. We detect an infrared excess in one of the systems, indicating that accretion from a circumstellar debris disk is ongoing. The main-sequence progenitor mass of this star was $4.8 \pm 0.2\,M_{\odot}$, demonstrating that rocky, differentiated planets may form around short-lived B-type stars.

The accurate astrometry of the Gaia mission[7] enabled the identification of nearby, intrinsically faint white dwarfs against much more numerous luminous background stars[8], and spectroscopic observations of practically all 524 northern white dwarfs within 40 pc are now complete[9]. We have detected absorption of the lithium 6,708 Å doublet in the spectra of three cool (effective temperature $T_{\rm eff} < 5{,}000$ K) white dwarfs (Fig. 1) within this sample (LHS 2534, WD J231726.74+183052.75 and WD J182458.45+121316.82), revealing the presence of this lithophile element within their photospheres.

The 6,708 Å doublet of neutral lithium is the only strong transition of this element at optical wavelengths, and because of the low ionization energy of lithium (5.4 eV), it becomes rapidly undetectable in hotter white dwarfs. Inspecting the published spectroscopy of cool white dwarfs at distances beyond 40 pc (refs. [10,11]), we identified a fourth system (SDSS J133001.17+643523.69) that exhibits lithium absorption.

Spectroscopy of planetary bodies accreted into the pristine hydrogen or helium atmospheres of white dwarfs provides direct measurements of their bulk abundances[2], similar to the analysis of meteorites to determine the composition of Solar System planets[12]. All four stars with photospheric lithium also exhibit sodium and calcium lines (Fig. 1), enabling a comparative study of the volatile and refractory content of their accreted planetesimals. The planetesimals, or fragments thereof, are most probably scattered via gravitational interactions with more massive bodies from distances of several astronomical units into the tidal disruption radius of the white dwarf[13]. An alternative way of delivering planetary material to the white dwarf is the Kozai–Lidov mechanism in wide binaries[14]; however, we do not detect wide companions for any of the four stars discussed here in Gaia Data Release 2 (DR2).

The observational data available for these objects were analysed using a model atmosphere code that has been specifically developed to correctly treat the complex physics in the high-density atmospheres of white dwarfs[15]. We fitted $T_{\rm eff}$ and the stellar radius using published broadband photometry and parallax (Methods and Extended Data Fig. 1), and subsequently determined the photospheric abundances using spectroscopy (Extended Data Fig. 2), with the procedure repeated until convergence (Extended Data Fig. 3). The analysis of LHS 2534 required additional effort as the star exhibits a magnetic field of 2.10 MG (Methods). We measured the atmospheric parameters and lithium, sodium and calcium abundances for all four stars, and also detected magnesium, potassium, chromium and iron in LHS 2534. The effective temperatures, $T_{\rm eff} = 3{,}350$–$4{,}780$ K, are among the lowest of any debris-accreting white dwarfs[10], reflecting the selection effect imposed by the neutral lithium detection.

We compare the abundance ratios of log(Li/Na) versus log(Ca/Na) of the four white dwarfs with those of the Sun[12], the bulk Earth[16], the continental crust[17] and CI chondrites[12] (Fig. 2a). All four objects reside within a cluster, with log(Ca/Na) between −1 and 0, and log(Li/Na) between −2.5 and −1. Owing to the rapid burning of lithium in the young Sun, the solar abundance is several orders of magnitude below those of the four white dwarfs and Solar System planetary compositions. The composition of the planetary debris within the four systems is noticeably enhanced in lithium and depleted in calcium with respect to the Solar System planetary benchmarks, and most closely resembles the abundances found in the continental crust. The unusually large log(Li/Na) and low log(Ca/Na) ratios can be partially explained via differential diffusion of metals out of the convection zones since the end of the accretion episode, caused by the different elemental sinking timescales.

We computed sinking timescales for each detected element[18] (Methods and Extended Data Fig. 4), and indicate the evolution of LHS 2534, WD J2317+1830 and WD J1824+1213 due to differential evolution in Fig. 2a (note the increased step sizes for WD J2317+1830 and WD J1824+1213). For LHS 2534, depending on how long ago accretion stopped, the parent body abundances could be consistent with those of the continental crust (~2 Myr ago (Ma)) or CI chondrites

[1]Department of Physics, University of Warwick, Coventry, UK. [2]Centre for Exoplanets and Habitability, University of Warwick, Coventry, UK. [3]Institut für Theoretische Physik und Astrophysik, University of Kiel, Kiel, Germany. [4]European Southern Observatory, Garching, Germany.
✉e-mail: M.Hollands.1@warwick.ac.uk

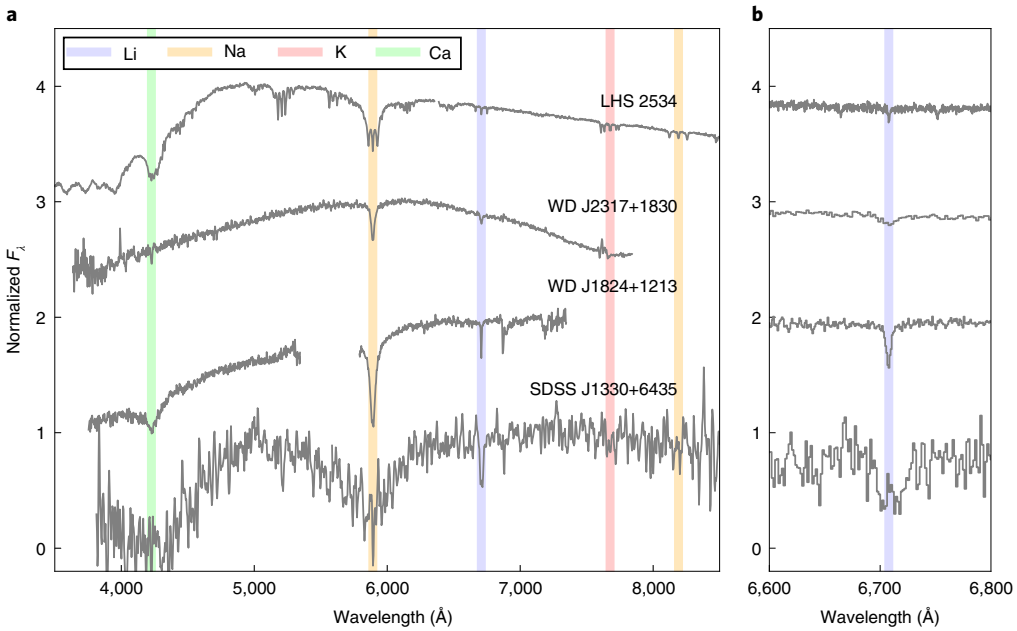

Fig. 1 | Optical spectra of the four white dwarfs with photospheric lithium. The wavelengths of the most important transitions are indicated by the coloured bars. F_λ is the intensity flux per unit wavelength. **a**, Spectra smoothed by a Gaussian with a full-width at half-maximum of 3 Å for clarity, with the exception of SDSS J1330+6435, for which 8 Å was used. **b**, Zoom-ins of the lithium doublet. Spectra are not smoothed.

(~3.5 Ma). At ~8 Ma, log(Ca/Na) values approach the bulk Earth value, but log(Li/Na) values would be about an order of magnitude too low. This degeneracy is broken by the additional detection of potassium in LHS 2534. The relative abundances of the alkali metals lithium, sodium and potassium are entirely incompatible with either those of bulk Earth or CI chondrites, independent of the accretion history (Fig. 2b). Instead, combined constraints from the lithium and potassium abundances are consistent with LHS 2534 having accreted a fragment of planetary crust around 2 Ma. Whereas the other three white dwarfs with photospheric lithium lack potassium detections, their close clustering near LHS 2534 in log(Li/Na) versus log(Ca/Na) strongly suggests that they, too, are contaminated by fragments of planetary crust. A similar analysis was possible for WD J1824+1213 and SDSS J1330+6435, although only considering log(Li/Na) versus log(Ca/Na) as potassium was not detected. Their past trajectories point closely towards the bulk Earth; however, this origin requires many diffusion timescales to have elapsed, necessitating extremely massive parent bodies. It is therefore much more probable that smaller parent bodies were more recently accreted[19] with compositions corresponding to particularly lithium-rich crust. WD J2317+1830 required a different analysis owing to its very short diffusion timescales.

To investigate the compositional diversity among cool white dwarfs, we selected three other cool white dwarfs (5,000–5,800 K) with published high-quality optical spectra that do not show the lithium 6,708 Å line[19] for comparison (SDSS J0744+4649, SDSS J0916+2540 and SDSS J1535+1247; Extended Data Fig. 5). We established upper limits for their photospheric lithium abundances and measured calcium and sodium abundances following the same methodology as outlined above. All three stars are distinctly offset from the cluster of lithium-rich white dwarfs in the log(Li/Na) versus log(Ca/Na) diagram (Fig. 2a). Their log(Ca/Na) values range from broadly resembling CI chondrites to a value exceeding that of bulk Earth. This corroborates our hypothesis that the four white dwarfs with photospheric lithium are accreting planetary debris with a clearly distinct crust-like composition.

Crust-like debris compositions have been suggested previously[5,19] on the basis of the detection of large calcium and aluminium abundances. However, both elements also have relatively high mass fractions within the mantle of a differentiated planet, and whereas the interpretation of calcium and aluminium-rich material as signatures of differentiation is certainly plausible[6], it does not support a definitive detection of crust fragments. In contrast, the mass fractions of the alkali metals lithium, potassium and sodium is one to two orders of magnitude higher in the Earth's continental crust than in its mantle[20], making them unambiguous tracers of planetary crusts.

Given that the photospheric abundances reflect the composition of the entire convection zone, in which the material remains homogeneously mixed, it is possible to estimate lower limits on the accreted planetary body masses. The properties of the outer convection zones (Extended Data Fig. 4) depend sensitively on the white dwarf mass and log(H/He) ratio, and vary only mildly as function of $T_{\rm eff}$ within the narrow range spanned by the four stars. The masses of the individual elements contained within the convection zones are reported in Extended Data Fig. 4. Scaling the sodium mass contained within the convection zone by its mass fraction of 2.4% in the continental crust of the Earth[17], we estimate the minimum masses of the crust fragments accreted into these white dwarfs to be in the range 5×10^{17}–3×10^{20} g. This compares with $\sim4\times10^{25}$ g for the Earth's continental crust[17], hence the observed level of atmospheric contamination requires only relatively small splinters of the crust of an Earth-like planet.

WD J2317+1830 has a small outer convection zone, owing to its large mass and mixed hydrogen/helium atmosphere (Extended Data Fig. 4). The sinking timescales within WD J2317+1830 are therefore on the order of thousands of years, much shorter than the millions of years typical of cool helium-atmosphere white dwarfs[21]. As accretion episodes are expected to last for 10^5–10^6 years (ref. [22]) it is therefore likely that WD J2317+1830 is still in the process of accreting from a circumstellar debris disk. This hypothesis is supported by the detection of an infrared excess (Fig. 3a), which is consistent (Methods) with a flat, passive, optically thick disk of dust heated by the white dwarf[1]. The infrared excess is detected in the UKIRT K and WISE W1 and W2 bands. For comparison, we selected 116

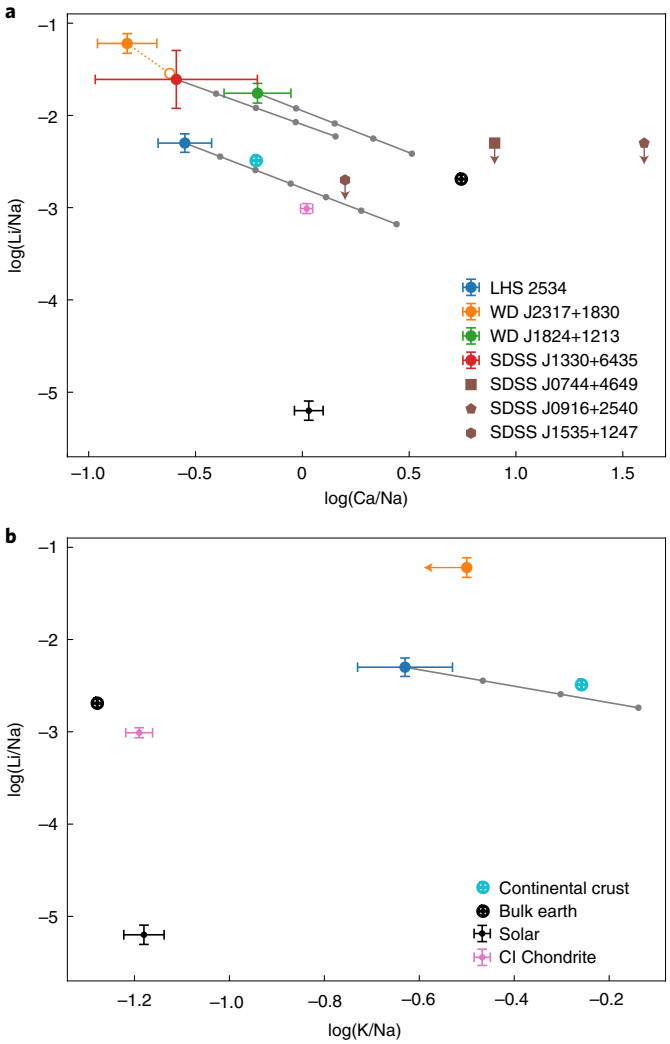

Fig. 2 | Number density abundance ratios of debris-accreting white dwarfs and Solar System benchmarks. a, The log(Li/Na) versus log(Ca/Na) ratios of the four white dwarfs with lithium detections (coloured circles) are enhanced with respect to the Earth's continental crust. The open orange point indicates the composition of the planetary body accreted by WD J2317+1830 assuming accretion–diffusion equilibrium. The grey lines illustrate the evolution of the photospheric abundances of the other three stars due to differential diffusion if accretion has stopped in the past. The dots on these tracks indicate steps of 1 Myr for LHS 2534 and 10 Myr for WD J1824+1213 and SDSS J1330+6435. Solar System benchmark compositions are shown for comparison, as well as three white dwarfs at which lithium has not been detected (brown symbols, arrows indicating upper limits for Li/Na). LHS 2534 has also photospheric potassium, and its log(Li/Na) versus log(Ca/Na) (**a**) and log(Li/Na) versus log(K/Na) (**b**) ratios are consistent with having accreted a fragment of planetary crust ~2 Ma. Error bars correspond to 1σ uncertainties. The legends apply to both panels.

white dwarfs within 130 pc of the Gaia DR2 white dwarf catalogue[8] and cross-matched them with WISE detections, with the further requirement of W1 − W2 uncertainties <0.05 mag. WD J2317+1830 is a clear outlier, presenting a 4σ excess in W1 − W2 (Fig. 3b). The proper motions for WD J2317+1830 measured from the WISE observations obtained from 2010 to 2016[23] agree with those determined by Gaia[7], corroborating the association of the WISE fluxes with the white dwarf. This places WD J2317+1830 as the coolest and oldest white dwarf known with a debris disk detection[24].

The infrared excess of the disk is $L_{IR}/L_{wd} = 0.06$, where L_{IR} and L_{wd} are the disk and white dwarf luminosities, respectively.

Assuming that WD J2317+1830 is in accretion–diffusion equilibrium[21], the mass flow rates through the bottom of the convection zone are identical to the accretion rates from the debris disk, which we compute (Methods) to be 760 g s^{-1}, 92,000 g s^{-1} and 37,000 g s^{-1} for lithium, sodium and calcium. Adopting the assumption that sodium accounts for 2.4% of the accreted mass (for continental crust abundances[17]) implies a total accretion rate of $\sim 3 \times 10^6$ g s^{-1}, broadly in agreement with the expected rate driven by the low Poynting–Robertson drag exercised by this cool white dwarf on the dust[25] and is consistent with the rates observed for other accreting systems (10^5–10^{11} g s^{-1})[26]. These estimates do not account for three-dimensional effects within convective white dwarf envelopes, and recent work[27] suggests that these effects may result in higher accretion rates than found from the one-dimensional calculations we used.

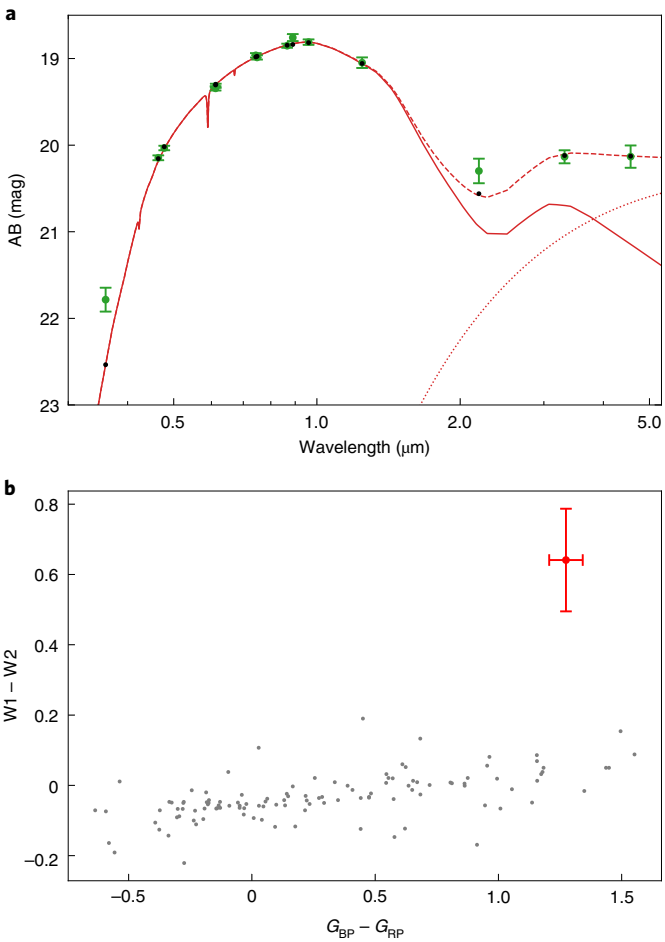

Fig. 3 | An infrared excess at WD J2317+1830. a, Our best fitting white dwarf model (solid curve) for WD J2317+1830 is shown with the photometry from SDSS, Pan-STARRS, UKIRT and WISE (green circles with error bars), showing a flux excess in the K, W1 and W2 bands. An opaque, optically thick disk heated by the white dwarf[1] with an inclination of 70° and an inner-edge temperature of 1,500 K (dotted line), when combined with the white dwarf flux (dashed line) provides a good fit to the photometry. **b**, WD J2317+1830 clearly stands out with an unusually red W1 − W2 colour when compared with white dwarfs with similar Gaia $G_{BP} - G_{RP}$ colour (grey points, from a cross-match of Gaia white dwarfs[8] with WISE and W1 − W2 uncertainties <0.05 mag). Error bars correspond to 1σ uncertainties.

There are few undisputed detections of planets with host star masses $\geq 3.1\,M_{\odot}$ (refs. [28,29]). Using the empirical initial-to-final mass relation[30], the high mass of WD J2317+1830 provides a probable indication that main-sequence stars as heavy as $4.8 \pm 0.2\,M_{\odot}$, corresponding to B-type stars, form planetary systems and that they survive to white dwarf stage. Note that despite the relatively short main-sequence lifetime of the progenitor, second-generation planet formation can largely be ruled out, as lithium burning on the main sequence would result in lithium-poor planetesimals, unlike those observed here. WD J2317+1830 is also one of the oldest systems known to have formed differentiated rocky planets, with a cooling age of 9.5 ± 0.2 Gyr and total age of 9.7 ± 0.2 Gyr. These mass and age measurements provide constraints for planet formation models that are extremely difficult to achieve from observations of planets around main-sequence or giant stars[29], and the detection of a debris disk at WD J2317+1830 demonstrates that planetary systems, or what is left of them, can remain dynamically active for practically the age of the Galaxy.

Lithium enrichment of giant stars has been interpreted in previous works as the result of the accretion of giant planets engulfed during the red giant phase[31] and lithium has been identified in the atmosphere of a giant exoplanet via transmission spectroscopy[32]. The detection of lithium within white dwarf photospheres originating from the accretion of planetary crust fragments represents an important link to the overall evolution of planetary systems, providing the sensitivity to establish the composition of the crusts of differentiated rocky planets.

Methods

Identification and observations. Three of the stars with lithium detections were found among our observations of white dwarfs within 40 pc (ref. [9]), whereas the fourth was identified from its Sloan Digital Sky Survey (SDSS) spectrum[11].

LHS 2534 is a nearby white dwarf located 38 pc away, and represents the first discovered magnetic metal-contaminated white dwarf[33]. The Zeeman effect from the 2.1 MG magnetic field[10] splits the photospheric lines into multiple components. For most transitions (where fine structure interactions are much weaker than that of the magnetic field), this results in three components separated by 98.0 cm^{-1} (46.686 $\mathrm{cm}^{-1}\,\mathrm{MG}^{-1}$ in general). On 2019 January 14 we obtained spectra of LHS 2534 using X-Shooter, an intermediate resolution echelle spectrograph mounted on the Very Large Telescope at Paranal. Two exposures of 1,250 s each were taken in the UVB and visible arms, with 1.0 and 0.9 arcsec slit widths, respectively. All data were reduced using the standard procedures within the REFLEX (version 2.9.1, http://www.eso.org/sci/software/esoreflex) reduction tool developed by the European Southern Observatory (ESO). Telluric line removal was performed on the reduced spectra using MOLECFIT[34,35] (version 1.1.0). The X-Shooter spectra clearly reveal the Li I 6,708 Å line Zeeman split into three components, where the depths of the π and σ components reach 0.14 and 0.10 of the continuum, respectively.

We observed WD J2317+1830 on 2018 September 2 using the OSIRIS spectrograph on the Gran Telescopio Canarias (GTC) during service mode observations as part of our International Time Programme (ID ITP08). We used the R1000B grating with a 1 arcsec slit width providing a resolving power of ~1,000 as measured from the sky spectrum. Debiasing, flat-fielding and extraction of the 1D spectra were performed using packages from the Starlink collection of software (version 2018A). Wavelength and flux calibration were performed using Molly (version 1.1.7, http://deneb.astro.warwick.ac.uk/phsaap/software/). As the service mode flux standards were observed with a wider slit width (2.5 arcsec), the quality of flux calibration and telluric removal were generally poor, although this did not affect the quality of our subsequent fits, as the continuum is well defined. The two strongest features of the spectrum were the Na I 5,893 Å doublet and the Li I 6,708 Å doublet (Fig. 1). The Ca I 4,227 Å line was also detected, although it was much weaker.

WD J1824+1213 was observed on 2018 August 7 and 8, again as part of our ITP, using the Intermediate-dispersion Spectrograph and Imaging System (ISIS) mounted on the William Herschel Telescope (WHT). We used the R600B and R600R gratings with a slit width varying between 1–1.5 arcsec between the two nights, and employing 2 × 2 binning, resulting in an average resolution of ~2 Å. The spectrum exhibits an almost saturated Na I doublet, a narrow Li 6,708 Å doublet and a relatively broad Ca I 4,227 Å line (Fig. 1).

Given the detection of lithium in three cool white dwarfs, we investigated the published spectroscopy of metal-contaminated objects with similar temperatures and identified the Li I 6,708 Å line in the SDSS spectrum of SDSS J1330+6435[11]. SDSS J1330+6435 was recently revisited in ref. [36], in which the lithium absorption feature is visible in one of the figures, although the authors did not comment on the presence of photospheric lithium.

The detection of photospheric lithium in the SDSS spectrum of SDSS J1330+6435 raised the possibility that other cool white dwarfs with lithium lines in their SDSS spectroscopy may have hitherto gone unnoticed. We therefore carried out a search for lithium-bearing cool white dwarfs, extracting the 37,259 white dwarf candidates with SDSS spectroscopy from the Gaia DR2 white dwarf catalogue[8]. We removed 7,396 objects that were classified by the authors as quasars on the basis of their SDSS spectroscopy.

We ran an automated search on the 29,863 remaining spectra, which (simply put) involved fitting a Gaussian profile at the expected wavelength of the Li I 6,708 Å line, and then measuring the significance. More specifically, we clipped each spectrum to the range 6,610–6,810 Å, which we then normalized via a fit with a first-order polynomial, excluding the region 6,690–6,730 Å. At the low resolution of the SDSS spectroscopy ($R \approx 2{,}000$), the Li I 6,708 Å doublet is not resolved, and we therefore fitted it with a Gaussian with a width of $\sigma = 5$ Å, where the amplitude of the Gaussian was the only free parameter. Given the width of the Gaussian, even large radial velocity shifts of 200 $\mathrm{km\,s}^{-1}$ are contained well within the fitted profile. We visually inspected all spectra where the amplitude parameter was measured to a significance of $>5\sigma$ in the direction of absorption, and where the reduced χ^2 was less than 2.0.

This process easily recovered SDSS J1330+6435 with an amplitude of 7.3σ and a reduced $\chi^2 = 1.033$. After removing multiple false positives (mostly magnetic hydrogen-atmosphere white dwarfs with $B \approx 7$ MG where the σ^+ component coincides with Li I 6,708 Å), we did not identify any other white dwarfs with conclusive lithium absorption.

Atmospheric analysis. The spectra and available photometry were analysed using the Koester LTE model atmosphere code[15]. Some improvements to the code have been implemented since its use in previous publications, several of which are relevant to this work. Improvements to the equations of state have been made to accommodate the very cool nature of these stars (WD J1824+1213 in particular). A unified profile for the Ca I 4,227 Å resonance line broadened by neutral helium is also now used. Our calculations used the potentials and dipole moments provided by T. Leininger and recently presented with similar profile calculations[37].

For the photometric fitting, we made use of a wide range of photometry (Extended Data Fig. 1). This included, wherever available, Pan-STARRS[38], SDSS[39] and SkyMapper[40] in the optical. In the infrared, we used 2MASS[41,42], UKIRT[43–45] and WISE[46]. Note that for the latter, we made use of the recent catWISE catalogue[23], which provides W1 and W2 detections for all four stars discussed here.

Before the photometric fit, we converted all magnitudes to the AB scale. However, we chose to exclude the Gaia photometry, because when using the provided AB zero points, we found consistent disagreement with other optical photometric surveys (that is SDSS, Pan-STARRS and Skymapper, which were always found to be mutually in agreement). In addition to the main parameters of $T_{\rm eff}$ and radius, the parallax is included as a dummy parameter, with the Gaia values serving as Gaussian priors. This has the desired effect of correctly folding the parallax uncertainty into our radius estimates, and to some extent into the $T_{\rm eff}$ estimates. The hydrogen and metal abundances were included in the models used in the photometric fits, although their values were fixed (to become free parameters for the spectroscopic fitting, where $T_{\rm eff}$ and the radius are fixed instead). The model fluxes, $F_\nu(\lambda)$, where F_ν is flux per unit frequency and λ is wavelength, were scaled by the radius and parallax, and synthetic AB magnitudes, m, were calculated from

$$\langle F_\nu \rangle = \frac{\int \mathrm{d}\lambda\, F_\nu(\lambda) S(\lambda)/\lambda}{\int \mathrm{d}\lambda\, S(\lambda)/\lambda}, \quad (1)$$

and

$$m = -2.5 \log_{10}(\langle F_\nu \rangle / 3{,}631), \quad (2)$$

where $S(\lambda)$ is the energy-counting filter response curve and F_ν is in units of Jy. The atmospheric parameters were then fitted via χ^2 minimization between the observed and synthetic magnitudes. For these nearby white dwarfs, the effects of interstellar reddening can be considered negligible. An important caveat regards the photometric uncertainties, which for some of the deep surveys such as Pan-STARRS, can be as small as a few millimag. These data tend to dominate the fit, and result in unrealistically small uncertainties (<10 K on $T_{\rm eff}$). It is therefore important to note that these photometic data may have a relative precision at the millimag level, particularly when derived from stacked multi-epoch observations; however, the absolute fluxes have additional systematic uncertainties. To account for this, we added a constant systematic uncertainty to all available photometry of a given object. The magnitude of this systematic uncertainty was varied until the best fit had a reduced χ^2 of one. We found values of ~0.04 mag were required for LHS 2534, WD J2317+1830 and WD J1824+1213. SDSS J1330+6435 is sufficiently faint (the photometric errors are sufficiently large) that this step was not necessary.

For the spectroscopic fitting, we used fixed $T_{\rm eff}$ and radius values derived from the photometric fit. The surface gravity, log$g$, was calculated from $T_{\rm eff}$ and the radius using the white dwarf mass–radius relation[47]. For LHS 2534 and

SDSS J1330+6435 where the atmospheric hydrogen content is trace at most, we adopted the thin hydrogen mass–radius relation, whereas for WD J2317+1830 and WD J1824+1213 (which have mixed hydrogen/helium atmospheres), we used the thick hydrogen relation instead. The flux calibration of our spectroscopy is of variable quality, therefore for WD J2317+1830 and WD J1824+1213 (where the continuum is well defined), at each step in the least-squares fit, we performed a local normalization of the data, fitting a spline to the ratio of the observed spectrum and the model to rescale the spectral fluxes. For LHS 2534 and SDSS J1330+6435, we instead recalibrated the spectral fluxes against the available optical photometry, fitting the difference between observed and synthetic photometry with second-order polynomials.

These spectroscopic and photometric fits were then iteratively repeated until convergence was found between the two solutions. The abundance errors obtained from the covariance matrix of the spectroscopic fits only considered the statistical uncertainty around a fixed $T_{\rm eff}$, and so were typically unrealistically too small (for example, <0.03 dex). The spectroscopic fits were therefore repeated with the best-fit $T_{\rm eff}$ increased by 1σ, with the subsequent shift in abundances added in quadrature to the statistical uncertainties.

Further details for each object are summarized in the following subsections, including any departures from the general approach described above. The final results for all four white dwarfs are compiled in Extended Data Fig. 2. The best-fit models to each of the stars are shown in Extended Data Fig. 3.

Analysis of LHS 2534. As the brightest of our four objects, LHS 2534 has a multitude of photometry, covering its entire spectral energy distribution (SED). However, the main challenge to fitting this object is its 2.1 MG magnetic field. Our models are intrinsically non-magnetic, therefore to improve the accuracy of our fits within this limitation, we triplicated the majority of spectral lines, reducing the loggf values (oscillator strengths) by $\log_{10}(3)$ for each component. Exceptions are the Ca II and Mg II resonance lines, for which we used precomputed unified line profiles.

With the higher-resolution spectroscopic data, we immediately determined that the Zeeman triplet located between 5,100 Å and 5,300 Å was in fact not from Mg I (ref. [33]), but rather Cr I as the central component has a rest-frame (air) wavelength of 5,207 Å. However, we note that the σ^+ component of Mg I may have been visible at 5,155 Å with its other components blended with Cr I. The magnesium abundance was further constrained from the red wing of the 2,852 Å Mg I resonance line. Other notable spectral features were K I lines (discussed below), Zeeman split lines from the Na I 8,191 Å doublet and a complex splitting pattern from the Ca II 8,600 Å triplet.

As well as lithium, for LHS 2534, we detected potassium from Zeeman split K I lines. We did not detect this element for any of the other objects; however, we note that for WD J1824+1213 our wavelength coverage did not extend red enough, and for SDSS J1330+6435 the spectrum was of too poor a quality to infer the presence of K I lines. For WD J2317+1830, we were instead able to obtain an upper limit. Future observations may therefore also reveal potassium in these stars. Confirming that the six components observed around 7,680 Å (Supplementary Fig. 1) did belong to K I was complicated by the fact that the interaction of the 2.1 MG magnetic field is comparable to the fine-structure energy separation of the K I doublet. For much smaller fields, the doublet components will be split into four and six sub-components, according to the anomalous Zeeman effect. In higher fields, where the spin–orbit interaction is disrupted, three components separated by $\mu_{\rm B}B$ would be observed instead, where B is magnetic field strength and $\mu_{\rm B}$ is the Bohr magneton. The 2.10 MG field falls into the intermediate regime, instead observing a triplet of doublets (Supplementary Fig. 1). To determine the wavelengths empirically, the energies of the upper levels can be found from the eigenvalues of

$$\begin{pmatrix} E_1+2\beta & 0 & 0 & 0 & 0 & 0 \\ 0 & E_1+\frac{2}{3}\beta & 0 & 0 & \frac{\sqrt{2}}{3}\beta & 0 \\ 0 & 0 & E_1-\frac{2}{3}\beta & 0 & 0 & \frac{\sqrt{2}}{3}\beta \\ 0 & 0 & 0 & E_1-2\beta & 0 & 0 \\ 0 & \frac{\sqrt{2}}{3}\beta & 0 & 0 & E_2+\frac{1}{3}\beta & 0 \\ 0 & 0 & \frac{\sqrt{2}}{3}\beta & 0 & 0 & E_2-\frac{1}{3}\beta \end{pmatrix}, \quad (3)$$

where $E_1 = 13{,}042.90\,{\rm cm}^{-1}$ and $E_2 = 12{,}985.19\,{\rm cm}^{-1}$ (the energies of the unperturbed $^2P_{3/2}$ and $^2P_{1/2}$ respectively), and $\beta = 46.686\,{\rm cm}^{-1}\,{\rm MG}^{-1}\,B$. Because the lower $^2S_{1/2}$ level (the potassium ground state) has no orbital angular momentum, the perturbed energies of the two sub-states are simply $\pm\beta$. Valid transitions can be found according to the normal selection rules, that is $\Delta m_j = 0, \pm 1$ and $\Delta m_s = 0$, where m_j and m_s are the z-components of the total and spin angular momenta, respectively. Setting B to 2.10 MG, we determined the wavelengths of the six allowed transitions, finding excellent agreement with the observed data (Supplementary Fig. 1), thus confirming the transitions belong to potassium.

We started our fits by adopting published parameters[10]. Within the least-squares fit to the spectrum, we found that we required a moderate hydrogen abundance, allowing for a better match to the continuum slope redward of 5,000 Å, which was too steep for our initial hydrogen abundance of log(H/He) = −5, and also a better match to the flux level blueward of 4,000 Å. Some of the metal lines in our the spectrum are much narrower than we were able to reproduce in our models (the cores of the Na I 5,892 Å and the Na I 8,191 Å doublet, the lithium and potassium lines, the Cr I lines and the many Zeeman-split components of the Ca II 8,600 Å triplet) unless the hydrogen abundance was raised to log(H/He) ≈ −1, although this came at the expense of substantially reducing the fit quality to other spectral features, in particular the Ca I 4,227 Å resonance line. Because the measurement of lithium and potassium abundances are crucial to our discussion, we instead optimized those elements to match the equivalent width. We discuss the narrowness of lithium lines in particular below.

From our fit to the photometry we derived a $T_{\rm eff}$ somewhat cooler than found in previous analyses[10,33,48]. However, those studies were performed before the release of Gaia DR2 astrometry, which places an additional constraint on the radius (and therefore mass and log$g$). We note that at the higher temperature of 5,200 K found in a previous analysis[10], we are forced to consider a log$g$ of 8.22, whereas our $T_{\rm eff}$ of $4{,}780 \pm 50$ K requires a more typical surface gravity of 7.97. Furthermore, at the higher temperature we also required a hydrogen abundance closer to log(H/He) = −1 to suppress the level of flux bluewards of 4,000 Å, although (as noted above) such a hydrogen abundance causes problems fitting other features of the spectrum. Because we computed non-magnetic models, as with all cool metal-contaminated white dwarfs, we find convection up to the photosphere. However, it has been found that magnetic fields can inhibit convective processes[49], which is probably the case for LHS 2534, since we derive a plasma β parameter value of ∼0.5 in the photosphere[50], indicating that magnetic pressure dominates over thermal pressure. However, calculating our models without convection results in only minor changes to the emergent spectrum. Furthermore, we emphasize that with such a marginally low plasma β value, convective velocities are damped by less than one order of magnitude. These convective velocities are still large compared with microscopic diffusion velocities[27], suggesting that metals are still efficiently mixed, similarly to the non-magnetic case.

Analysis of WD J2317+1830. For this white dwarf photometry is available from SDSS, Pan-STARRS, UKIRT and WISE. The UKIRT J magnitude is from the UKIRT Hemisphere Survey (UHS)[45], with the K band from the Wide-field nearby Galaxy-cluster survey (WINGS)[43,44]. The SDSS band is poorly fitted in Extended Data Fig. 3, although the detection flags indicate that the uncertainty is underestimated in this filter[39]. The combination of UKIRT and WISE photometry reveal collision-induced absorption (CIA) is present in the atmosphere of this star.

We found that it was not possible to fit all the near-infrared photometry simultaneously. Instead, we used only the optical and J-band photometry to constrain $T_{\rm eff}$ and the radius. This produced a much more consistent fit with spectroscopy, where the width of the Na doublet and y − J colour are both sensitive to the He/H ratio. As is evident from Extended Data Fig. 3, this results in too low a flux in the K and WISE bands. We noted that the W1 − W2 colour is far too flat compared with the expected Rayleigh–Jeans tail. For two photometric measurements along a Rayleigh–Jeans tail, it is expected that

$$\frac{m_2 - m_1}{\log_{10}(\lambda_2/\lambda_1)} \simeq 5 \quad (4)$$

where $m_{1,2}$ are the two AB magnitudes, and $\lambda_{1,2}$, their corresponding central wavelengths. For example, for the W1/2 photometry of LHS 2534, equation (4) is evaluated to be 4.7 ± 0.8, whereas for WD J2317+1830 the same quantity is 0.0 ± 1.1—more than 4σ smaller than the expected value for a Rayleigh–Jeans slope. We highlight this excess in Fig. 3b, where we show the W1 − W2 colour against the $G_{\rm BP} - G_{\rm RP}$ colour for WD J2317+1830 and a cross-match of the Gaia white dwarf catalogue[8] and WISE photometry[51,52]. Initially this cross-match contained 70,050 sources. We further refined this by keeping only sources with white dwarf probabilities $P_{\rm wd} > 0.75$, reducing the sample to 28,333. From a colour–colour diagram of $G_{\rm RP} - {\rm W1}$ versus $G_{\rm BP} - G_{\rm RP}$ it was clear that the cross-match was contaminated by a larger number of sources with very red $G_{\rm RP} - {\rm W1}$ (that is, flux contamination from nearby sources, white dwarfs with main-sequence companions). We therefore made a cut of $G_{\rm RP} - {\rm W1} > 0.2 + 1.3(G_{\rm BP} - G_{\rm RP})$, leaving only the main white dwarf locus, containing 4,076 objects. Finally, we removed objects with W1 − W2 uncertainties >0.05 mag, leaving only the 116 objects shown in Fig. 3b, all of which are contained within 130 pc.

We considered the possibility that the perceived flux excess of WISE photometry result from contamination by another object located within the large WISE point spread function. However, the catWISE[23] photometry collected over the period 2010–2016 shows that the source detected by WISE has a proper motion consistent with that measured by Gaia, strongly arguing against background contamination. Furthermore, the excess is also seen in the UKIRT K band, which has a much better spatial resolution.

A possible explanation that could resolve the discrepancy between the observed SED and the model spectra would be a modification of the CIA absorption profiles, as they have been subject to limited observational tests. While simply increasing the strength of the absorption would extend the red wing of the H_2–He opacity into the W1 band, this would also result in excess absorption in the K band. However, the H_2–He CIA opacity has been shown[53] to be distorted at the high densities relevant to these stars (>0.1 g cm^{-3}). The opacity table used in this work has only

temperature dependence and so it is feasible that density-dependent shifts may explain our observations. Even so, a strong argument against this comes from the fact that we were able to fit WD J1824+1213 accurately in all photometric passbands, despite this star having stronger CIA due to its lower $T_{\rm eff}$.

A more natural explanation is that the infrared excess arises from a circumstellar dust disk irradiated by the white dwarf. Using the simple flat disk model[1], we found that a reasonable fit is obtained for an inner disk temperature of ∼1,500 K, an outer temperature of <500 K and an inclination of ∼70° (dashed curves in Fig. 3a and Extended Data Fig. 3). The fact that WD J2317+1830 has short diffusion timescales, which make it likely that we observe the star actively accreting, corroborates the detection of an infrared excess as the signature of a dusty debris disk, formed from the tidal disruption of a planetesimal.

In addition to LHS 2534, the spectrum of WD J2317+1830 also covers the wavelength region of the potassium doublet. Strong telluric absorption coincides with the wavelength of the blue component, making it impossible to extract a meaningful upper limit from this line—even with telluric removal (as in Fig. 1), large residuals remain. The red component resides outside the region covered by telluric absorption, and so we were able to use this line to establish an upper limit of log(K/He) < −10.5. This results in an abundance ratio upper limit of log(K/Na) < −0.5. Since this is higher than the measurement of LHS 2534 (Fig. 2b), the true value for WD J2317+1830 could be several 0.1 dex below the upper limit and be broadly consistent with the location of LHS 2534 in Fig. 2b.

Analysis of WD J1824+1213. For this object, optical photometry are available from Pan-STARRS, although because of the 1,200 mas yr^{-1} proper motion, it appears as four separate detections, where we list the weighted averages provided in Extended Data Fig. 1. Additionally, WD J1824+1213 has a UKIRT J-band detection in the UHS[45]. WD J1824+1213 was found to be an ultra-cool white dwarf ($T_{\rm eff}$ = 3,350 ± 50 K) with a mixed H/He atmosphere similar to WD J2317+1830. This results in very strong CIA from H_2–He, to the extent that its effect is measurable from only the Pan-STARRS $z-y$ colour, although it is further constrained by the J band. W1 and W2 magnitudes were also found within the catWISE data, and agree well with our best fitting model, despite the very strong CIA. The most notable features in the spectral data are the near-saturated sodium and calcium lines, the latter of which shows a reasonable fit with our unified profile.

Analysis of SDSS J1330+6435. This stellar remnant has been recently modelled[36] owing to its extremely strong and broad sodium absorption. Although the unified sodium line profile used in that analysis is not currently implemented in our models, we were able to obtain an adequate fit to the data.

Using the SDSS and Pan-STARRS photometry, we found a $T_{\rm eff}$ and log$g$ lower than that derived in the earlier analysis[36]. Regardless, our model synthetic photometry is mostly in good agreement with the data, although we note that our model slightly under-predicts the flux in the W1 band compared with the measurement.

Two spectra are available from SDSS, although the second spectrum (taken with the BOSS instrument) has a very poor signal-to-noise ratio. Even so, we decided to co-add these spectra to improve the spectroscopic uncertainties. From comparison with the photometry (Extended Data Fig. 1), the flux calibration of both spectra was found to be poor, therefore recalibration against the photometry (as described above) was required for each spectrum before they could be co-added. We found co-adding provided a modest boost in the signal-to-noise ratio of 10% in the red and 20% in the blue (relative to the better of the two spectra).

The main challenge in fitting this spectrum was measuring the calcium abundance. The calcium resonance line was modelled here using the aforementioned unified profile and yields a reasonable fit in Extended Data Fig. 3. However, we found that the calcium and magnesium abundances were highly anti-correlated—as the calcium resonance line is essentially saturated even at a low abundance, a similarly good fit to both the spectrum and u-band photometry can be achieved by lowering the calcium abundance and increasing the magnesium abundance. There is insufficient information that could constrain the Mg/Ca ratio, and so a higher-quality spectrum will be needed to measure these abundances independently. Therefore our adopted calcium abundance (Extended Data Fig. 2) assumes log(Mg/Ca) = 1.5 dex, which is the average value found in an earlier study[54].

We note that the sodium and calcium abundances that we determined are significantly lower than those in the previous analysis[36]. This difference arises from our lower $T_{\rm eff}$ measurement, resulting in a changed excitation balance. We therefore required much lower sodium and calcium abundances to produce the same strength lines. Even so, we find our Ca/Na ratio is consistent with the previous analysis (log(Ca/Na) = −0.6 ± 0.4 versus −0.3 ± 0.4 in the previous work). The remaining difference in the Ca/Na ratio (while already within 1σ uncertainty) could be attributed to the anti-correlation between calcium and magnesium as described above.

Given the highly pressure broadened Na doublet, it is clear that the atmosphere of SDSS J1330+6435 must be helium-dominated, although trace hydrogen could be present at some level. Our best fit was performed assuming log(H/He) = −6 dex, although we were still able to establish an upper limit. We found that up to −4 dex, the models looked close to identical, with a small amount of CIA appearing at 2 μm, but otherwise continuing to agree well with all available photometry, and spectroscopy. However, at −3 dex we found that CIA pushed down the infrared flux compared with the optical enough to be in disagreement with the WISE photometry. Furthermore, the Na doublet started to become narrower than observed in the spectrum. We thus adopted −4 dex as our upper limit for the hydrogen abundance.

Linewidths of lithium. In our initial attempts to derive abundances, we found that the lithium lines were systematically much narrower than predicted by our models. On its own, these narrow lines might suggest an interstellar origin[55]; however, there are multiple arguments against this. First, for LHS 2534 the lithium doublet is Zeeman split by the 2.1 MG magnetic field. Second, all objects apart from SDSS J1330+6435 are located within 40 pc of the Sun (SDSS J1330+6435 is located 87 ± 7 pc away) where interstellar absorption can be considered negligible. Finally, in all four objects the observed lithium lines—although much narrower than those in the models—are still broader than the instrumental resolution. We determined this by first measuring the spectral resolution at the location of the lithium doublet by determining the widths of sky emission lines in the sky spectrum. In each object, we then fitted the lithium doublet with a Voigt profile, with the Gaussian component σ fixed to the spectral resolution, and with the Lorentzian component, γ, as a free parameter. The results are given in Supplementary Table 1, and include the radial velocities measured from the Voigt profiles (not corrected for gravitational redshift). We thus conclude that in all four cases, the lines must be photospheric in origin.

Instead, we considered the possibility that the overly broad lines in our models arise from inaccurate atomic data (uncertainties can often be as large as a factor of 2–3 (0.3–0.5 dex). For lithium, we obtained atomic data from VALD[56,57], where the broadening constants log($\Gamma_{\rm rad}$), log($\Gamma_{\rm stark}/n_{\rm e}$), log($\Gamma_{\rm VdW}/n_{\rm H}$) were found to be 7.56, −5.78 and −7.57 respectively, where $\Gamma_{\rm rad}$ is the radiation broadening constant, $\Gamma_{\rm stark}$ is the broadening constant per electron number, $\Gamma_{\rm VdW}$ is the van der Waals broadening constant per neutral hydrogen number, $n_{\rm e}$ is the electron number density, and $n_{\rm H}$ is the neutral hydrogen number density. These broadening constants are nominally calculated for temperatures of 10,000 K and for a single perturber, and so internal scaling is required for different temperatures, densities and, in the case of neutral broadening, other perturbers such as He. In the cool, dense atmospheres of these four white dwarfs, the dominant line-broadening process is perturbations by neutral particles (that is hydrogen, helium, H_2). Indeed, we found that the lithium linewidths in all objects are sensitive to adjustments in the neutral-broadening constant. We therefore decided to empirically determine a correction to the neutral-broadening constant, log($\Gamma_{\rm VdW}/n_{\rm H}$), from our observations.

We decided to perform this measurement on a single object, comparing the other three stars for consistency. We chose WD J1824+1213 as the calibration object because its γ measurement has the highest relative precision (Supplementary Table 1). Furthermore WD J1824+1213 has the second highest γ/σ ratio; γ/σ is higher for SDSS J1330+6435, but the low signal-to-noise ratio and other challenges in fitting this object make it a poor choice of calibrator.

We generated a grid of models with log($\Gamma_{\rm VdW}/n_{\rm H}$), spanning −9.0 to −8.0 in steps of 0.1 dex, and log(Li/H) spanning −12.50 to −11.00 in 0.25 dex steps. Other atmospheric parameters ($T_{\rm eff}$, log$g$, other abundances), were set to the best-fitting values in Extended Data Fig. 2. The optimal broadening constant was determined via a nonlinear least-squares fit to the data, interpolating the models (convolved by the 1.9 Å instrumental broadening) at arbitrary abundance/log($\Gamma_{\rm VdW}/n_{\rm H}$). We found the best fitting value to be log($\Gamma_{\rm VdW}/n_{\rm H}$) = −8.53 ± 0.06 or, in other words, a change of −0.96 ± 0.06 dex.

The best-fitting models for all four white dwarfs with the revised broadening constant are displayed in red in Supplementary Fig. 2. For comparison, models with the original broadening constant are shown in orange, although with abundances revised upwards by 0.3 dex for clarity. Naturally, the improvement for WD J1824+1213 is exemplary, given that this object was used for calibration, although the linewidth for WD J2317+1830 (which has a similar derived atmospheric H/He ratio) was also found to show good agreement when using the revised values. LHS 2534 and SDSS J1330+6435, which both have He-dominated atmospheres, show improvement compared with the original broadening constant (where the lithium lines are completely washed out), although the lines remain far wider than observed in the data. The remaining discrepancy is particularly pronounced for LHS 2534, although other lines in the spectrum of this object are also found to be narrower than expected. This includes the potassium lines (Supplementary Fig. 1), and the 5,892 and 8,191 Å doublets of sodium. The Na I 5,892 Å lines are particularly noteworthy, because we were able to accurately fit their wings (Extended Data Fig. 3), while narrow cores remain that we are unable to fit with our models. Since we have no trouble fitting these sodium lines in the other three objects, we take this as evidence that the 2.1 MG magnetic field has a strong effect on the atmospheric structure, exacerbating the narrowness of weaker lines. Indeed, we find that the gas pressure in our models is $10^{10.5}$ dyn cm^{-2}, whereas the magnetic pressure must be $10^{11.2}$ dyn cm^{-2} given the 2.10 MG magnetic field. Therefore, in addition to only adjusting the lithium lines, for this object, it was also

necessary to reduce the neutral broadening constants for Cr I and K I by the same amount to better estimate the photospheric abundances.

Although we clearly find improvement with the revised broadening constant, similar issues are not encountered in other cool stellar atmospheres with lithium lines—for instance the solar atmosphere and those of giant stars. However, calculations of giant star atmosphere models with the reduced neutral broadening constant show no discernible difference in the linewidth (M. Steffen, personal communication), indicating that other broadening processes dominate within those atmospheres.

White dwarf masses and evolution. For two of the stars in our sample, WD J1824+1213 and SDSS J1330+6435, we derive particularly small masses ($0.28 \pm 0.03\,M_{\odot}$ and $0.38 \pm 0.06\,M_{\odot}$, respectively). These masses are presumed to be unrealistic, as the Galaxy is too young to produce such low-mass white dwarfs, and are representative of the challenges common to modelling cool white dwarfs[58] with $T_{\rm eff}$<5,000 K. In fact, extremely low masses are commonly derived for white dwarfs with strong CIA absorption[59] and imply missing opacity in the stellar models. Such difficulties are often understood to arise from strongly wavelength-dependent opacities such as CIA[53] and the red wing of Lyman α (ref. [60]).

Our models include CIA opacities[61–64] from H_2–H, H_2–He, H_2–H_2, H–He and He–He–He. We also include broadening[65] of Lyα by H_2. However, we do not include the effects of pressure distortion in the H_2–He opacity[53]. Although we do not have access to these specific data, their inclusion in our models may go some of the way to explain these low masses. The expectation is therefore that these stars have higher true $T_{\rm eff}$ than from our analysis, which would therefore allow for smaller radii, needed to remain consistent with the photometry and parallaxes, which (via the mass–radius relation for white dwarfs) implies higher masses.

In the following, we assume that the derived luminosities (Extended Data Fig. 2) of WD J1824+1213 and SDSS J1330+6435 are correct as they provide an adequate fit to the photometric SED, and we also assume that the mass is drawn from the distribution found for warmer white dwarfs[66]; that is, $M = 0.614 \pm 0.122\,M_{\odot}$. For WD J1824+1213, we obtain $T_{\rm eff} = 4{,}050^{+260}_{-240}$ K and a sinking timescale $\tau = 9.41^{+0.35}_{-0.95}$ Gyr for thick hydrogen layers, which are appropriate for the large total hydrogen mass in the star. For SDSS J1330+6435, again assuming $M = 0.614 \pm 0.122\,M_{\odot}$ leads to $T_{\rm eff} = 4{,}160^{+290}_{-270}$ K and $\tau = 7.54^{+0.31}_{-0.60}$ Gyr for thin hydrogen layers. Clearly both white dwarfs have long cooling times, but it is not possible to estimate the main-sequence lifetime owing to the uncertainty on the mass.

For WD J1824+1213 (the most extreme case of the low-mass/low-$T_{\rm eff}$ systems), we refitted the photometry and spectrum with the $T_{\rm eff}$ fixed to 4,050 K (as described above), and with the radius and atmospheric abundances as free parameters, to see if this provided an adequate solution, which could be the case if our low-mass solution was simply a local minimum. Although the best model for this restricted fit did (by design) result in a mass close to $0.6\,M_{\odot}$, we found that the model failed to accurately reproduce the shape of the SED in the both the optical and infrared, showing particular disagreement in the J band of around 0.5 mag. Therefore, we rule out a second minimum in the parameter space at higher $T_{\rm eff}$, although this does not discount the possibility that improved atmospheric models may shift the best solution to higher temperatures and thus towards more reasonable masses. Even so, the consistency in the abundance ratios of WD J1824+1213 and SDSS J1330+6435 compared with LHS 2534 and WD J2317+1830 (Fig. 2) indicates that our conclusions on a crust origin for the accreted material is unaffected in these two low mass systems. We note that forcing an increased $T_{\rm eff}$ shifts the optimal abundances: log(H/He) was reduced by about 0.3 dex with all metal abundances increased by 0.5–0.6 dex. The similarity in metal abundance shifts implies that the location of WD J1824+1213 in Fig. 2a is largely unaffected by systematic uncertainty in $T_{\rm eff}$.

For LHS 2534 we derive a mass of $0.55 \pm 0.02\,M_{\odot}$ corresponding cooling age of 5.8 ± 0.2 Gyr. We expect the magnetic field to have negligible influence on cooling age[50]. Such a white dwarf mass implies a very long main-sequence lifetime, possibly longer than the cooling time[67]. It is possible that LHS 2534 is also impacted by the model systematics mentioned above, and therefore we refrain from estimating a total age.

In contrast, our fit to WD J2317+1830 reveals a mass of $1.00 \pm 0.02\,M_{\odot}$ and cooling age of 9.5 ± 0.2 Gyr, making it the among most massive white dwarfs detected with signatures of a planetary system[29]. The large mass implies a massive progenitor with a relatively small main-sequence lifetime, leading to a precise total age of 9.7 ± 0.2 Gyr using an empirical initial-to-final mass relation[30] and main-sequence lifetimes[68].

Kinematics and population membership. Although we could establish a reliable total age for only one of the four analysed white dwarfs, kinematics can be useful to identify population membership[69–71]. In Supplementary Table 2, we rely on the precise Gaia astrometry to derive tangential velocities as well as motion in Galactic coordinates U, V and W. We had to assume zero radial velocity as this quantity is poorly constrained from our spectroscopic observations. In earlier studies of halo white dwarf candidates[69], a 2σ halo membership required $|U| > 94\,{\rm km\,s^{-1}}$ or $V > 60\,{\rm km\,s^{-1}}$ or $V < -130\,{\rm km\,s^{-1}}$. Using the same requirements, only WD J1824+1213 is a halo white dwarf candidate, as previously identified[71], although all our objects have relatively large tangential velocities, suggesting an old disk population[72], consistent with the large cooling ages.

The chemical abundances in these old white dwarfs have the potential to provide constraints on planet formation around stars formed in the early history of the Galaxy, and hence possibly under metal-poor conditions. However, early disk membership is not necessarily linked to progenitors of significant sub-solar metallicity[73,74], and further insight will require a larger sample of cool, debris-accreting white dwarfs.

Sinking times. We used our new envelope code[18] to determine convection zone sizes and sinking timescales[21] for each element considered in our sample. With only four objects, we were able to use the best-fit atmospheric models discussed in the previous sections as boundary conditions on the upper envelope for self-consistency (as opposed to interpolating a grid of models). These results are listed in Extended Data Fig. 4. Using these timescales, it is possible to trace back the atmospheric abundance histories of a metal Z (with sinking timescale τ and elapsed time since accretion t) using

$$\log({\rm Z/He})(t) = \log({\rm Z/He})(0) + \frac{t}{\ln(10)\tau}, \tag{5}$$

implying that the relative abundances for two elements evolves as

$$\log({\rm Z_1/Z_2})(t) = \log({\rm Z_1/Z_2})(0) + \frac{t}{\ln(10)}\left[\tau_1^{-1} - \tau_2^{-1}\right]. \tag{6}$$

The convection zone masses, combined with our abundance measurements (Extended Data Fig. 2), allow us to determine the mass of each element mixed within the convection zones, providing lower limits on the amounts of accreted material (Extended Data Fig. 4). In the case of WD J2317+1830, where accretion–diffusion equilibrium has been assumed, the elemental diffusion fluxes (equal to the elemental accretion rates) can be calculated by dividing the respective convection zone masses by their corresponding diffusion timescales.

Data availability

The data that support the plots within this paper and other findings of this study are available from the ESO science archive facility, the GTC public archive, ING archive and SDSS database; or from the corresponding author upon reasonable request.

Code availability

The Koester model atmosphere and envelope codes are not publicly available, although details of their internal operation and input physics can be consulted from ref. [15].

Received: 24 July 2020; Accepted: 16 December 2020;
Published online: 11 February 2021

References

1. Jura, M. A tidally disrupted asteroid around the white dwarf G29-38. *Astrophys. J. Lett.* **584**, L91–L94 (2003).
2. Zuckerman, B., Koester, D., Melis, C., Hansen, B. M. & Jura, M. The chemical composition of an extrasolar minor planet. *Astrophys. J.* **671**, 872–877 (2007).
3. Gänsicke, B. T. et al. The chemical diversity of exo-terrestrial planetary debris around white dwarfs. *Mon. Not. R. Astron. Soc.* **424**, 333–347 (2012).
4. Doyle, A. E., Young, E. D., Klein, B., Zuckerman, B. & Schlichting, H. E. Oxygen fugacities of extrasolar rocks: evidence for an Earth-like geochemistry of exoplanets. *Science* **366**, 356–359 (2019).
5. Zuckerman, B. et al. An aluminum/calcium-rich, iron-poor, white dwarf star: evidence for an extrasolar planetary lithosphere? *Astrophys. J.* **739**, 101 (2011).
6. Bonsor, A. et al. Are exoplanetesimals differentiated? *Mon. Not. R. Astron. Soc.* **492**, 2683–2697 (2020).
7. Gaia Collaboration et al. Gaia Data Release 2—summary of the contents and survey properties. *Astron. Astrophys.* **616**, A1 (2018).
8. Gentile Fusillo, N. P. et al. A Gaia Data Release 2 catalogue of white dwarfs and a comparison with SDSS. *Mon. Not. R. Astron. Soc.* **482**, 4570–4591 (2019).
9. Tremblay, P. E. et al. Gaia white dwarfs within 40 pc: I. Spectroscopic observations of new candidates. *Mon. Not. R. Astron. Soc.* **497**, 130–145 (2020).
10. Hollands, M. A., Koester, D., Alekseev, V., Herbert, E. L. & Gänsicke, B. T. Cool DZ white dwarfs: I. Identification and spectral analysis. *Mon. Not. R. Astron. Soc.* **467**, 4970–5000 (2017).
11. Harris, H. C. et al. An initial survey of white dwarfs in the Sloan Digital Sky Survey. *Astron. J.* **126**, 1023–1040 (2003).
12. Lodders, K. Solar system abundances and condensation temperatures of the elements. *Astrophys. J.* **591**, 1220–1247 (2003).

13. Debes, J. H., Walsh, K. J. & Stark, C. The link between planetary systems, dusty white dwarfs, and metal-polluted white dwarfs. *Astrophys. J.* **747**, 148 (2012).
14. Petrovich, C. & Muñoz, D. J. Planetary engulfment as a trigger for white dwarf pollution. *Astrophys. J.* **834**, 116 (2017).
15. Koester, D. White dwarf spectra and atmosphere models. *Mem. Soc. Astron. Ital.* **81**, 921–931 (2010).
16. McDonough, W. in *Earthquake Thermodynamics and Phase Transformation in the Earth's Interior* (eds Teisseyre, R. & Majewski, E.) 5–24 (Elsevier, 2000).
17. Rudnick, R. L. & Gao, S. in *Treatise on Geochemistry* Vol. 3, 1–56 (Elsevier, 2003).
18. Koester, D., Kepler, S. O. & Irwin, A. W. New white dwarf envelope models and diffusion—application to DQ white dwarfs. *Astron. Astrophys.* **635**, A103 (2020).
19. Hollands, M. A., Gänsicke, B. T. & Koester, D. Cool DZ white dwarfs II: compositions and evolution of old remnant planetary systems. *Mon. Not. R. Astron. Soc.* **477**, 93–111 (2018).
20. Lodders, K. & Fegley, B. Jr *Chemistry of the Solar System* (RSC, 2011).
21. Koester, D. Accretion and diffusion in white dwarfs. New diffusion timescales and applications to GD 362 and G 29-38. *Astron. Astrophys.* **498**, 517–525 (2009).
22. Girven, J. et al. Constraints on the lifetimes of disks resulting from tidally destroyed rocky planetary bodies. *Astrophys. J.* **749**, 154 (2012).
23. Eisenhardt, P. R. M. et al. The CatWISE preliminary catalog: motions from WISE and NEOWISE data. *Astrophys. J. Suppl.* **247**, 69 (2020).
24. Debes, J. H. et al. A 3 Gyr white dwarf with warm dust discovered via the Backyard Worlds: Planet 9 citizen science project. *Astrophys. J. Lett.* **872**, L25 (2019).
25. Rafikov, R. R. Metal accretion onto white dwarfs caused by Poynting-Robertson drag on their debris disks. *Astrophys. J. Lett.* **732**, L3 (2011).
26. Farihi, J. Circumstellar debris and pollution at white dwarf stars. *New Astron. Rev.* **71**, 9–34 (2016).
27. Cunningham, T., Tremblay, P.-E., Freytag, B., Ludwig, H.-G. & Koester, D. Convective overshoot and macroscopic diffusion in pure-hydrogen-atmosphere white dwarfs. *Mon. Not. R. Astron. Soc.* **488**, 2503–2522 (2019).
28. Sato, B. et al. Substellar companions to seven evolved intermediate-mass stars. *Publ. Astron. Soc. Jpn* **64**, 135 (2012).
29. Veras, D. et al. Constraining planet formation around 6-8 $M_{\odot}$ stars. *Mon. Not. R. Astron. Soc.* **493**, 765–775 (2020).
30. Cummings, J. D., Kalirai, J. S., Tremblay, P. E., Ramirez-Ruiz, E. & Choi, J. The white dwarf initial-final mass relation for progenitor stars from 0.85 to 7.5 $M_{\odot}$. *Astrophys. J.* **866**, 21 (2018).
31. Aguilera-Gómez, C., Chanamé, J., Pinsonneault, M. H. & Carlberg, J. K. On lithium-rich red giants. I: engulfment of substellar companions. *Astrophys. J.* **829**, 127 (2016).
32. Chen, G. et al. The GTC exoplanet transit spectroscopy survey. IX: detection of haze, Na, K, and Li in the super-Neptune WASP-127b. *Astron. Astrophys.* **616**, A145 (2018).
33. Reid, I. N., Liebert, J. & Schmidt, G. D. Discovery of a magnetic DZ white dwarf with Zeeman-split lines of heavy elements. *Astrophys. J. Lett.* **550**, L61–L63 (2001).
34. Smette, A. et al. Molecfit: a general tool for telluric absorption correction. I: method and application to ESO instruments. *Astron. Astrophys.* **576**, A77 (2015).
35. Kausch, W. et al. Molecfit: a general tool for telluric absorption correction. II: quantitative evaluation on ESO-VLT/X-Shooterspectra. *Astron. Astrophys.* **576**, A78 (2015).
36. Blouin, S. et al. A new generation of cool white dwarf atmosphere models: III. WD J2356-209: accretion of a planetesimal with an unusual composition. *Astrophys. J.* **872**, 188 (2019).
37. Blouin, S., Allard, N. F., Leininger, T., Gadéa, F. X. & Dufour, P. Line profiles of the calcium I resonance line in cool metal-polluted white dwarfs. *Astrophys. J.* **875**, 137 (2019).
38. Chambers, K. C. et al. The Pan-STARRS1 Surveys. Preprint at https://arxiv.org/abs/1612.05560 (2016).
39. Alam, S. et al. The eleventh and twelfth data releases of the Sloan Digital Sky Survey: final data from SDSS-III. *Astrophys. J. Suppl.* **219**, 12 (2015).
40. Wolf, C. et al. SkyMapper southern survey: first data release (DR1). *Proc. Astron. Soc. Aust.* **35**, e010 (2018).
41. Cutri, R. M. et al. *2MASS All-Sky Catalog of Point Sources (Cutri+ 2003)* II/246 (VizieR Online Data Catalog, 2003).
42. Skrutskie, M. F. et al. The Two Micron All Sky Survey (2MASS). *Astron. J.* **131**, 1163–1183 (2006).
43. Valentinuzzi, T. et al. WINGS: a wide-field nearby galaxy-cluster survey. III: deep near-infrared photometry of 28 nearby clusters. *Astron. Astrophys.* **501**, 851–864 (2009).
44. Moretti, A. et al. WINGS data release: a database of galaxies in nearby clusters. *Astron. Astrophys.* **564**, A138 (2014).
45. Dye, S. et al. The UKIRT Hemisphere Survey: definition and J-band data release. *Mon. Not. R. Astron. Soc.* **473**, 5113–5125 (2018).
46. Cutri, R. M. et al. *AllWISE Data Release (Cutri+ 2013)* II/328 (VizieR Online Data Catalog, 2013).
47. Fontaine, G., Brassard, P. & Bergeron, P. The potential of white dwarf cosmochronology. *Publ. Astron. Soc. Pac.* **113**, 409–435 (2001).
48. Hollands, M. A., Gänsicke, B. T. & Koester, D. The incidence of magnetic fields in cool DZ white dwarfs. *Mon. Not. R. Astron. Soc.* **450**, 681–690 (2015).
49. Gentile Fusillo, N. P. et al. Can magnetic fields suppress convection in the atmosphere of cool white dwarfs? A case study on WD2105-820. *Mon. Not. R. Astron. Soc.* **473**, 3693–3699 (2018).
50. Tremblay, P. E. et al. On the evolution of magnetic white dwarfs. *Astron. J.* **812**, 19 (2015).
51. Wright, E. L. et al. The Wide-field Infrared Survey Explorer (WISE): mission description and initial on-orbit performance. *Astron. J.* **140**, 1868–1881 (2010).
52. Mainzer, A. et al. Preliminary results from NEOWISE: an enhancement to the Wide-field Infrared Survey Explorer for solar system science. *Astrophys. J.* **731**, 53 (2011).
53. Blouin, S., Kowalski, P. M. & Dufour, P. Pressure distortion of the H_2-He collision-induced absorption at the photosphere of cool white dwarf stars. *Astrophys. J.* **848**, 36 (2017).
54. Blouin, S. Magnesium abundances in cool metal-polluted white dwarfs. *Mon. Not. R. Astron. Soc.* **496**, 1881–1890 (2020).
55. Ferlet, R. & Dennefeld, M. Interstellar lithium and the ^{7}Li/^{6}Li ratio in diffuse clouds. *Astron. Astrophys.* **138**, 303–310 (1984).
56. Ryabchikova, T. A., Piskunov, N. E., Kupka, F. & Weiss, W. W. The Vienna Atomic Line Database: present state and future development. *Balt. Astron.* **6**, 244–247 (1997).
57. Ryabchikova, T. et al. A major upgrade of the VALD database. *Phys. Scr.* **90**, 054005 (2015).
58. McCleery, J. et al. Gaia white dwarfs within 40 pc. II: the volume-limited Northern Hemisphere sample. *Mon. Not. R. Astron. Soc.* **499**, 1890–1908 (2020).
59. Kilic, M. et al. The 100 pc white dwarf sample in the SDSS footprint. *Astrophys. J.* **898**, 84 (2020).
60. Kowalski, P. M. & Saumon, D. Found: the missing blue opacity in atmosphere models of cool hydrogen white dwarfs. *Astrophys. J. Lett.* **651**, L137–L140 (2006).
61. Karman, T. et al. Update of the HITRAN collision-induced absorption section. *Icarus* **328**, 160–175 (2019).
62. Borysow, A., Jorgensen, U. G. & Zheng, C. Model atmospheres of cool, low-metallicity stars: the importance of collision-induced absorption. *Astron. Astrophys.* **324**, 185–195 (1997).
63. Borysow, A., Jorgensen, U. G. & Fu, Y. High-temperature (1000-7000 K) collision-induced absorption of H_2 pairs computed from the first principles, with application to cool and dense stellar atmospheres. *J. Quant. Spectrosc. Radiat. Transf.* **68**, 235–255 (2001).
64. Kowalski, P. M. Infrared absorption of dense helium and its importance in the atmospheres of cool white dwarfs. *Astron. Astrophys.* **566**, L8 (2014).
65. Rohrmann, R. D., Althaus, L. G. & Kepler, S. O. Lyman α wing absorption in cool white dwarf stars. *Mon. Not. R. Astron. Soc.* **411**, 781–791 (2011).
66. Tremblay, P.-E., Ludwig, H.-G., Steffen, M. & Freytag, B. Spectroscopic analysis of DA white dwarfs with 3D model atmospheres. *Astron. Astrophys.* **559**, A104 (2013).
67. Marigo, P. et al. Carbon star formation as seen through the non-monotonic initial-final mass relation. *Nat. Astron.* **4**, 1102–1110 (2020).
68. Hurley, J. R., Pols, O. R. & Tout, C. A. Comprehensive analytic formulae for stellar evolution as a function of mass and metallicity. *Mon. Not. R. Astron. Soc.* **315**, 543–569 (2000).
69. Oppenheimer, B. R., Hambly, N. C., Digby, A. P., Hodgkin, S. T. & Saumon, D. Direct detection of galactic halo dark matter. *Science* **292**, 698–702 (2001).
70. Seabroke, G. M. & Gilmore, G. Revisiting the relations: galactic thin disc age-velocity dispersion relation. *Mon. Not. R. Astron. Soc.* **380**, 1348–1368 (2007).
71. Kilic, M. et al. The age of the galactic stellar halo from Gaia white dwarfs. *Mon. Not. R. Astron. Soc.* **482**, 965–979 (2019).
72. Fantin, N. J. et al. The Canada-France imaging survey: reconstructing the Milky Way star formation history from its white dwarf population. *Astrophys. J.* **887**, 148 (2019).
73. Feltzing, S., Holmberg, J. & Hurley, J. R. The solar neighbourhood age-metallicity relation—does it exist? *Astron. Astrophys.* **377**, 911–924 (2001).
74. Casagrande, L. et al. New constraints on the chemical evolution of the solar neighbourhood and galactic disc(s). Improved astrophysical parameters for the Geneva-Copenhagen Survey. *Astron. Astrophys.* **530**, A138 (2011).

Acknowledgements

M.A.H. and P.-E.T. acknowledge useful discussions with H.-G. Ludwig and M. Steffen regarding neutral broadening of lithium lines. We also acknowledge J. McCleery for maintaining a database of 40 pc white dwarf spectra. M.A.H. and D.K. acknowledge atomic data from T. Leininger used for the Ca I unified profile. This research received funding from the European Research Council under the European Union's Horizon 2020 research and innovation programme number 677706 (WD3D). B.T.G. was supported by the UK STFC under grant number ST/T000406/1 and a Leverhulme Research Fellowship. Funding for the Sloan Digital Sky Survey IV (www.sdss.org) was provided by the Alfred P. Sloan Foundation, the US Department of Energy Office of Science and the participating institutions. Based on observations collected at the European Organisation for Astronomical Research in the Southern Hemisphere under ESO programme 0102.C-0351. This article is based on observations (programme ITP08) made in the Observatorios de Canarias del IAC with the WHT operated on the island of La Palma by the Isaac Newton Group of Telescopes in the Observatorio del Roque de los Muchachos and with the Gran Telescopio Canarias (GTC), installed at the Spanish Observatorio del Roque de los Muchachos of the Instituto de Astrofísica de Canarias, on the island of La Palma.

Author contributions

M.A.H. performed data reduction, analysis and interpretation and wrote the majority of the text. P.-E.T. and B.T.G. contributed to the data interpretation and writing of the article. D.K. developed the model atmosphere code used for the analysis. N.P.G.-F. contributed to the data reduction and analysis of photometric data.

Competing interests

The authors declare no competing interests.

Additional information

Extended data is available for this paper at https://doi.org/10.1038/s41550-020-01296-7.

Supplementary Information The online version contains supplementary material available at https://doi.org/10.1038/s41550-020-01296-7.

Correspondence and requests for materials should be addressed to M.A.H.

Peer review information *Nature Astronomy* thanks the anonymous reviewers for their contribution to the peer review of this work.

Reprints and permissions information is available at www.nature.com/reprints.

Publisher's note Springer Nature remains neutral with regard to jurisdictional claims in published maps and institutional affiliations.

© The Author(s), under exclusive licence to Springer Nature Limited 2021

Parameter	LHS 2534	WD J2317+1830	WD J1824+1213	SDSS J1330+6435
Ra	12:14:56.754	23:17:26.701	18:24:58.152	13:30:00.897
Dec	−02:34:09.34	+18:30:45.74	+12:13:00.11	+64:35:23.35
ϖ [mas]	26.19 ± 0.15	26.45 ± 0.50	25.47 ± 0.25	11.57 ± 0.93
$\mu_\alpha \cos(\delta)$ [mas/yr]	$+358.23 \pm 0.35$	-34.78 ± 1.02	-280.65 ± 0.40	-112.79 ± 3.06
μ_δ [mas/yr]	-419.28 ± 0.20	-452.49 ± 0.50	$-1,078.60 \pm 0.40$	-21.94 ± 1.80
Gaia $G_{\rm BP}$	18.277 ± 0.011	19.951 ± 0.062	19.381 ± 0.043	20.981 ± 0.211
Gaia G	17.824 ± 0.002	19.378 ± 0.005	18.554 ± 0.003	20.758 ± 0.015
Gaia $G_{\rm RP}$	17.249 ± 0.007	18.677 ± 0.028	17.741 ± 0.013	19.802 ± 0.073
Pan-STARRS g	18.221 ± 0.010	20.033 ± 0.013	19.504 ± 0.003	21.441 ± 0.065
Pan-STARRS r	17.772 ± 0.001	19.315 ± 0.009	18.551 ± 0.003	20.810 ± 0.047
Pan-STARRS i	17.614 ± 0.002	18.987 ± 0.011	18.046 ± 0.006	20.081 ± 0.025
Pan-STARRS z	17.573 ± 0.013	18.852 ± 0.009	17.927 ± 0.001	19.952 ± 0.030
Pan-STARRS y	17.536 ± 0.013	18.811 ± 0.023	17.999 ± 0.008	19.802 ± 0.070
SDSS u	20.870 ± 0.064	21.784 ± 0.136		25.192 ± 0.661
SDSS g	18.331 ± 0.007	20.146 ± 0.017		21.551 ± 0.059
SDSS r	17.746 ± 0.006	19.344 ± 0.012		20.860 ± 0.037
SDSS i	17.549 ± 0.007	18.963 ± 0.013		20.098 ± 0.031
SDSS z	17.509 ± 0.017	18.378 ± 0.034		19.782 ± 0.077
SkyMapper g	18.166 ± 0.015			
SkyMapper r	17.691 ± 0.027			
SkyMapper i	17.581 ± 0.021			
SkyMapper z	17.475 ± 0.041			
2MASS J	16.736 ± 0.155			
2MASS H	16.695 ± 0.283			
UKIRT J		18.129 ± 0.057	18.000 ± 0.046	
UKIRT K		18.420 ± 0.140		
WISE $W1$	16.423 ± 0.038	17.461 ± 0.072	17.443 ± 0.073	17.868 ± 0.074
WISE $W2$	16.429 ± 0.108	16.820 ± 0.127	17.174 ± 0.167	18.012 ± 0.285

Extended Data Fig. 1 | Astrometry and photometry for the four lithium-rich white dwarfs. Pan-STARRS, SDSS and SkyMapper photometry are given in the AB-system, with the remainder in the Vega system. Positions are given in the J2015.5 epoch.

Parameter	LHS 2534	WD J2317+1830	WD J1824+1213	SDSS J1330+6435
$T_{\rm eff}$ [K]	$4,780 \pm 50$	$4,210 \pm 50$	$3,350 \pm 050$	$3,660 \pm 50$
$\log g$	7.97 ± 0.04	8.64 ± 0.03	7.41 ± 0.07	7.65 ± 0.14
R [$\times 10^{-5} R_\odot$]	$1,269 \pm 29$	793 ± 21	$1,741 \pm 55$	$1,524 \pm 115$
M [$M_\odot$]	0.55 ± 0.02	1.00 ± 0.02	0.28 ± 0.03^a	0.38 ± 0.07^a
L [$\times 10^{-5} L_\odot$]	7.53 ± 0.13	1.78 ± 0.07	3.44 ± 0.09	3.82 ± 0.45
τ [Gyr]	5.8 ± 0.2	9.5 ± 0.2	5.5 ± 0.4	6.0 ± 1.0
B_s [MG]	2.10	-	-	-
log(H/He)	-3.19 ± 0.18	-0.09 ± 0.09	-0.07 ± 0.10	< -4
log(Li/He)	-11.83 ± 0.08	-11.19 ± 0.08	-11.95 ± 0.08	-11.96 ± 0.29
log(Na/He)	-9.53 ± 0.06	-9.96 ± 0.07	-10.19 ± 0.07	-10.35 ± 0.12
log(Mg/He)	-8.62 ± 0.06	-	-	-
log(K/He)	-10.16 ± 0.08	< -10.5	-	-
log(Ca/He)	-10.08 ± 0.11	-10.79 ± 0.12	-10.40 ± 0.14	-10.94 ± 0.36
log(Cr/He)	-10.28 ± 0.06	-	-	-
log(Fe/He)	-9.06 ± 0.08	-	-	-

Notes: (a) These masses are almost certainly underestimates resulting from missing opacity sources in the model atmospheres.

Extended Data Fig. 2 | Atmospheric parameters for the four white dwarfs with photospheric lithium. The abundances are in base 10 in terms of number ratio.

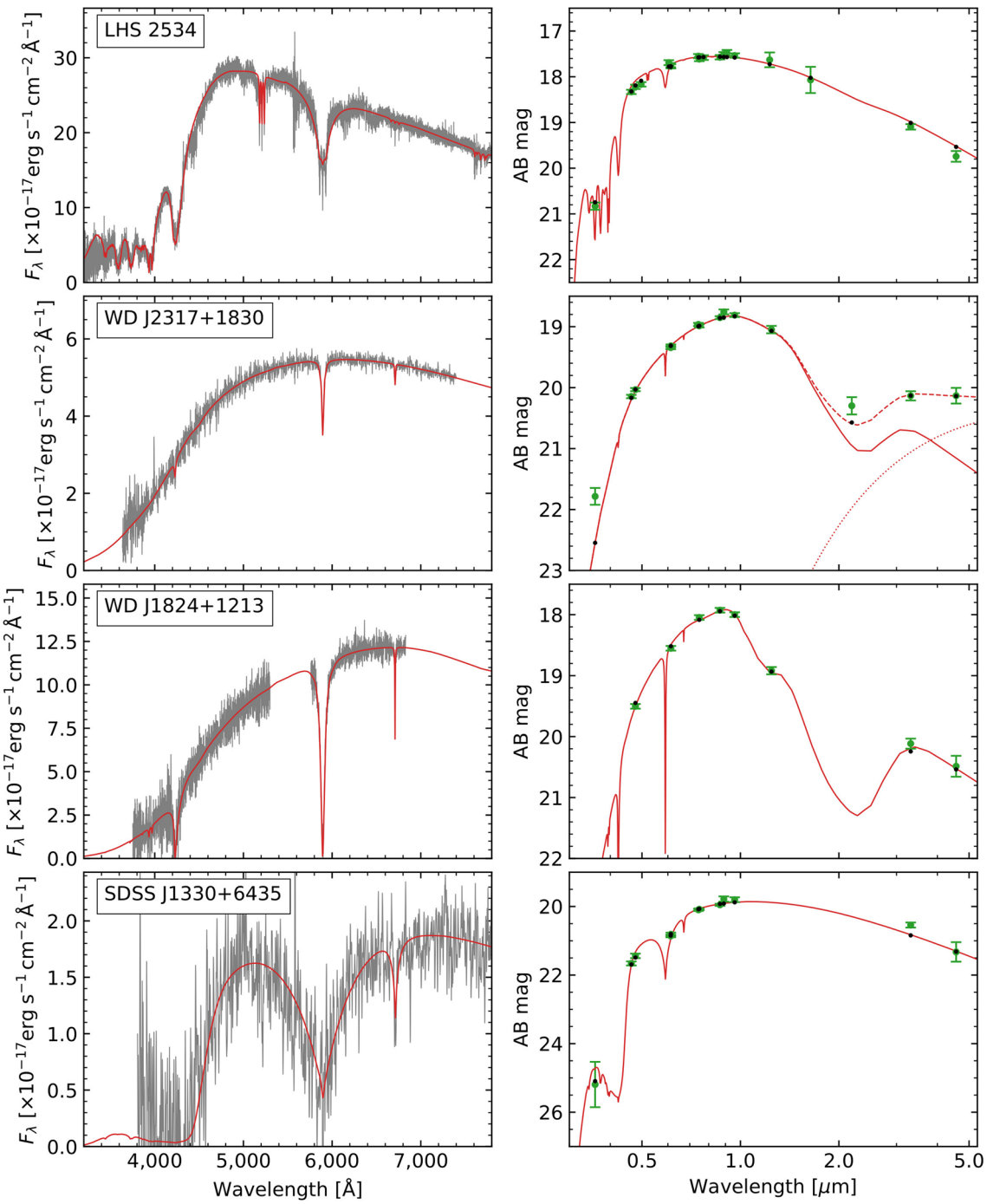

Extended Data Fig. 3 | Best fitting models compared with the spectra and photometry of the four lithium-bearing white dwarfs. In the right panel for WD J2317+1830, the disk model and white dwarf plus disk model are indicated by dotted and dashed curves, respectively. The spectrum of SDSS J1330+6435 has been smoothed with a Gaussian with a full width half maximum of 5 Å. Error bars correspond to 1σ uncertainties.

	LHS 2534	WD J2317+1830	WD J1824+1213	SDSS J1330+6435
$\log(M_{\rm cvz}/M_{\rm wd})$	-5.36	-7.88	-4.33	-4.36
H	(- , 9.59×10^{26})	(- , 4.35×10^{24})	(- , 2.55×10^{27})	(- , -)
Li	(3.59×10^{6}, 1.22×10^{16})	(9.79×10^{3}, 2.39×10^{14})	(2.12×10^{7}, 3.93×10^{16})	(3.50×10^{7}, 6.18×10^{16})
O	(2.43×10^{6}, -)	(6.26×10^{3}, -)	(1.61×10^{7}, -)	(2.43×10^{7}, -)
Na	(1.62×10^{6}, 8.06×10^{18})	(4.52×10^{3}, 1.34×10^{16})	(1.18×10^{7}, 7.49×10^{18})	(1.56×10^{7}, 8.28×10^{18})
Mg	(1.60×10^{6}, 6.88×10^{19})	(4.40×10^{3}, -)	(1.17×10^{7}, -)	(1.54×10^{7}, -)
Al	(1.41×10^{6}, -)	(3.98×10^{3}, -)	(1.05×10^{7}, -)	(1.34×10^{7}, -)
Si	(1.41×10^{6}, -)	(3.92×10^{3}, -)	(1.05×10^{7}, -)	(1.35×10^{7}, -)
K	(1.01×10^{6}, 3.22×10^{18})	(2.93×10^{3}, -)	(7.93×10^{6}, -)	(9.36×10^{6}, -)
Ca	(1.00×10^{6}, 3.98×10^{18})	(2.91×10^{3}, 3.45×10^{15})	(7.92×10^{6}, 8.05×10^{18})	(9.34×10^{6}, 3.71×10^{18})
Ti	(8.03×10^{5}, -)	(2.42×10^{3}, -)	(6.51×10^{6}, -)	(7.31×10^{6}, -)
Cr	(7.47×10^{5}, 3.24×10^{18})	(2.26×10^{3}, -)	(6.11×10^{6}, -)	(6.78×10^{6}, -)
Fe	(7.03×10^{5}, 5.82×10^{19})	(2.14×10^{3}, -)	(5.80×10^{6}, -)	(6.36×10^{6}, -)
Ni	(6.81×10^{5}, -)	(2.06×10^{3}, -)	(5.64×10^{6}, -)	(6.15×10^{6}, -)
crust	(- , 2.97×10^{20})	(- , 4.94×10^{17})	(- , 2.76×10^{20})	(- , 3.05×10^{20})

Extended Data Fig. 4 | White dwarf envelope parameters for our sample. The first row indicates the fractional convection zone mass. In subsequent rows, pairs correspond to the sinking timescale at the base of the convection zone in years, and (where abundances were determined) the elemental mass in the convection zone in g, i.e. (τ_Z/yr, m_Z/g). Diffusion timescales are given for all elements commonly considered in white dwarf planetary abundance studies. The final row, 'crust', provides estimates for the total material within the white dwarf convection zones, assuming a continental crust composition, scaled from the Na masses.

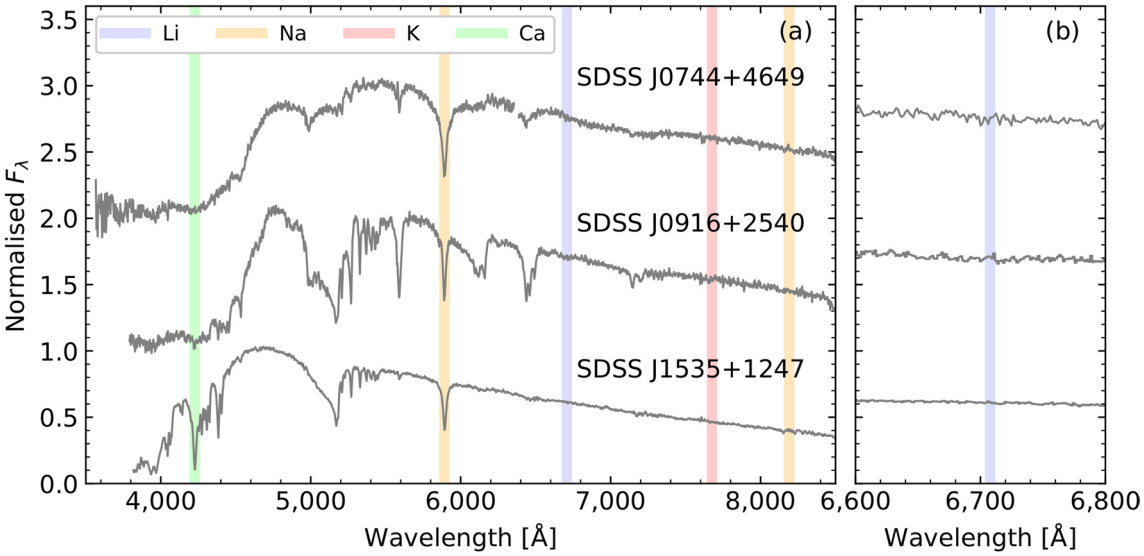

Extended Data Fig. 5 | SDSS spectra of three additional cool DZs with strong metal absorption features. Lithium lines are not detected for any of these stars. Spectra have been smoothed by a Gaussian with a full width half maximum of 3 Å for clarity.